Peak-Seeking Control Using Gradient and Hessian Estimates

John J. Ryan and Jason L. Speyer

***Abstract*— A peak-seeking control method is presented which utilizes a linear time-varying Kalman filter. Performance function coordinate and magnitude measurements are used by the Kalman filter to estimate the gradient and Hessian of the performance function. The gradient and Hessian are used to command the system toward a local extremum. The method is naturally applied to multiple-input multiple-output systems. Applications of this technique to a single-input single-output example and a two-input one-output example are presented.**

I. Introduction

Peak-seeking control, also referred to as extremum-seeking control, is concerned with on-line optimization across an unknown performance function of some physical system or process. Given noisy coordinate and magnitude measurements of the performance function, it attempts to move a plant to a local extremum. It has been studied in relation to many applications, such as formation flight for drag reduction [1], bio-reactors [2], and axial-flow compressor [3]. Peak-seeking control gained much attention in the 1950s and 1960s [4], [5], [6], [7] but interest in this field declined in the 1970s and 1980s. It has since had a resurgence of attention in the past 15 years [2], [8], [9].

In general, peak-seeking control methods can be divided into three categories: classical-gradient methods, parametric methods, and nonlinear methods. The classical-gradient methods estimate the performance function gradient using classical-control techniques and move the system accordingly [10]. Parametric methods parameterize the performance function to estimate the extremum position and move the system accordingly [1]. Nonlinear methods utilize nonlinear control techniques such as adaptive control and numerical optimization with line searches to estimate the gradient and move the system towards the extremum [11], [9].

The earliest work used classical-gradient methods partly due to ease of implementation in analog devices and the lack of inexpensive digital computers. The classical-gradient methods have recently been further developed in work by Ariyur [12], Krstic [13], and others who have developed a general design technique and proved local convergence of this approach [10]. The parametric methods are a newer approach. Some examples of work in this area are Najson [14], Chichka [1], Popovic [8]. Examples of nonlinear approaches can be found in [11] and [9].

This paper discusses a parametric method of peak-seeking control. It uses a linear time-varying Kalman filter to estimate the gradient and Hessian of the performance function and a Newton-method to drive the system toward an extremum. The paper is organized as follows. Section 2 provides an overview of the method. Section 3 discusses the Kalman filter design used to estimate the gradient and Hessian of the performance function. Section 4 presents a one-dimensional example and section 5 presents a two-dimensional example. Section 6 concludes the paper.

John Ryan is a Research Engineer at NASA DFRC and UCLA Graduate Student

Jason Speyer is a Professor of Mechanical and Aerospace Engineering at UCLA

II. Overview of Peak-Seeking Control Method

The goal of peak-seeking control is to move the position, $x(t)$, of a plant, P, to the extremum of a performance function $f\big(x(t)\big)$. Figure 1 displays this peak-seeking scheme's overall interconnection. Here, $x(t)$ is one of a number of states of P. Performance function magnitude may also affect the plant; in the figure, this is indicated by a dashed line. At a given iteration k, the difference between the current plant position, x_k, and the previous position, x_{k-1}, is calculated. The difference between the current performance function magnitude, $f(x_k)$, and the previous, $f(x_{k-1})$, is also calculated. These differences are used by a linear time-varying Kalman filter (KF) to estimate the current gradient, b_k, and Hessian, M_k. The gradient and Hessian are combined to form a position command, $x_c = b_k M_k^{-1}$, to drive the plant toward the performance function extremum. A filter (Filt) smoothes and scales the command to avoid providing P large step commands which can create unwanted actuator movements. A persistent excitation signal (PE) is added to the smoothed position command to ensure observability of the performance function. In practice, an initial position command initiates movement of the system. The plant is assumed to be stabilized by an inner-loop control.

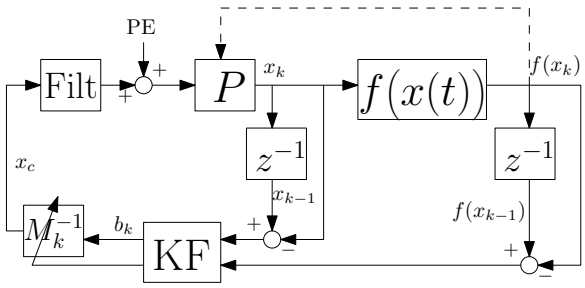

Fig. 1. Peak-seeking scheme interconnection

The method uses position measurements directly to estimate the gradient and Hessian. This requires the use of a linear time-varying Kalman filter. Use of a Kalman filter allows designers to utilize an array of Kalman filter design

techniques. This provides flexibility to the scheme and allows it to be applied to many problems.

III. Kalman Filter Design

Performance function gradient and Hessian are estimated using a linear time-varying Kalman filter whose states consist of elements at the current position. This is accomplished by parameterizing the performance function using first- and second-order terms of a Taylor series expansion.

Consider the Taylor series expansion of a performance function $f(x)$ about x_k

$$\begin{aligned} f(x) \approx f(x_k) + b_{x_k}^T (x - x_k) \\ + \frac{1}{2}(x - x_k)^T M_{x_k}(x - x_k) + o(x - x_k) \end{aligned} \tag{1}$$

where b_{x_k} is the gradient at x_k, M_{x_k} is the Hessian at x_k, and $o(\cdot)$ represents higher order terms. Evaluating (1) at x_{k-1} and rearranging yields

$$\Delta f_k = b_k^T \Delta x_k + \frac{1}{2}\Delta x_k^T M_{x_k} \Delta x_k \tag{2}$$

where $\Delta x_k = x_{k-1} - x_k$ and $\Delta f_k = f(x_{k-1}) - f(x_k)$. The higher-order terms have been dropped by assuming the performance function is adequately modeled as a quadratic function at any particular position.

For simplicity, we restrict ourselves to a two-dimensional case. Denote the positions in the two dimensions at time k as x_{1_k} and x_{2_k}. Denote the corresponding gradients as b_{1_k} and b_{2_k} and the corresponding Hessian as

$$M_k = \begin{bmatrix} M_{11_k} & M_{12_k} \\ M_{12_k} & M_{22_k} \end{bmatrix}.$$

Further denote

$$\begin{aligned} \Delta x_{1_k} &= x_{1_{k-1}} - x_{1_k} \\ \Delta x_{2_k} &= x_{2_{k-1}} - x_{2_k}. \end{aligned}$$

Equation (2) is then written as

$$\Delta f_k = \begin{bmatrix} \frac{1}{2}\Delta x_{1_k}^2 \\ \frac{1}{2}\Delta x_{2_k}^2 \\ \Delta x_{1_k}\Delta x_{2_k} \\ \Delta x_{1_k} \\ \Delta x_{2_k} \end{bmatrix}^T \begin{bmatrix} M_{11_k} \\ M_{22_k} \\ M_{12_k} \\ b_{1_k} \\ b_{2_k} \end{bmatrix}. \tag{3}$$

Equation (3) implies that a parameter estimation technique may be used to estimate the gradient and Hessian. Since the gradient and Hessian may change with x, and measurements of Δx_{1_k}, Δx_{2_k} and Δf_k may be noisy, a Kalman filter is an appropriate choice of estimator. The Kalman filter states are chosen to be

$$\zeta_k = \begin{bmatrix} M_{11_k} \\ M_{22_k} \\ M_{12_k} \\ b_{1_k} \\ b_{2_k} \end{bmatrix}.$$

This allows the measurement equation of a linear time-varying Kalman filter to take the form

$$\Delta f_k = H_k \zeta_k + v_k \tag{4}$$

where

$$H_k = \begin{bmatrix} \frac{1}{2}\Delta x_{1_k}^2 \\ \frac{1}{2}\Delta x_{2_k}^2 \\ \Delta x_{1_k}\Delta x_{2_k} \\ \Delta x_{1_k} \\ \Delta x_{2_k} \end{bmatrix}^T$$

and v_k represent a zero-mean Gaussian white-noise process with variance V_k.

The gradient and Hessian are modeled as a Brownian noise process since they may change in an unknown manner with x. The Kalman filter process equation is, therefore, given by

$$\zeta_{k+1} = I\zeta_k + w_k \tag{5}$$

where I is a 5×5 identity matrix and w_k represents a zero-mean Gaussian white-noise process with variance W_k.

The linear time-varying Kalman filter is implemented with the following equations:

$$\hat{P}_{k+1} = \bar{P}_k + W_k \tag{6a}$$

$$\zeta_{k+1} = \zeta_k + \bar{P}_k H_k^T V_k^{-1}(\Delta f_k - H_k \zeta_k) \tag{6b}$$

$$\bar{P}_k = (\hat{P}_k^{-1} + H_k^T V_k^{-1} H_k)^{-1} \tag{6c}$$

where $\bar{P}$ is the state covariance matrix, $\hat{P}$ the predicted state covariance matrix, and ζ the state vector. The values of W_k and V_k are used as tuning parameters. Typically, initial guesses of W_k and V_k are based on previously-obtained measurements of the noise or on a noise model. A trial-and-error process is then used to adjust the values in order to improve the estimates. Detailed derivations of the linear time-varying Kalman filter can be found in [15] and [16].

The Kalman filter may be expanded to include N measurements at each iteration k. Define

$$\Delta f_{k,n} = f(x_{1_k}, x_{2_k}) - f(x_{1_{k-n}}, x_{2_{k-n}}) \tag{7a}$$

$$\Delta x_{1_{k,n}} = x_{1_k} - x_{1_{k-n}} \tag{7b}$$

$$\Delta x_{2_{k,n}} = x_{2_k} - x_{2_{k-n}} \tag{7c}$$

and $v_{k,n}$ as the corresponding process noise. The index n takes values between 1 and N. The expansion is implemented by modifying the measurement equation (4) as

$$\begin{bmatrix} \Delta f_{k,1} \\ \Delta f_{k,2} \\ \vdots \\ \Delta f_{k,N} \end{bmatrix} = H_k \zeta_k + \begin{bmatrix} v_{k,1} \\ v_{k,2} \\ \vdots \\ v_{k,N} \end{bmatrix}. \tag{8}$$

Here

$$H_k = \begin{bmatrix} \frac{1}{2}\Delta x_{1_{k,1}}^2 & \frac{1}{2}\Delta x_{2_{k,1}}^2 & D_{k,1} & \Delta x_{1_{k,1}} & \Delta x_{2_{k,1}} \\ \frac{1}{2}\Delta x_{1_{k,2}}^2 & \frac{1}{2}\Delta x_{2_{k,2}}^2 & D_{k,2} & \Delta x_{1_{k,2}} & \Delta x_{2_{k,2}} \\ \vdots & \vdots & \vdots & \vdots & \vdots \\ \frac{1}{2}\Delta x_{1_{k,N}}^2 & \frac{1}{2}\Delta x_{2_{k,N}}^2 & D_{k,N} & \Delta x_{1_{k,N}} & \Delta x_{2_{k,N}} \end{bmatrix}$$

and $D_{k,n} = \Delta x_{1_{k,n}} \Delta x_{2_{k,n}}$. The process equation remains as it is shown in equation (5). The Kalman filter is implemented

as shown in equation (6) with

$$\Delta f_k = \begin{bmatrix} \Delta f_{k,1} \\ \Delta f_{k,2} \\ \vdots \\ \Delta f_{k,N} \end{bmatrix}$$

and

$$V_k = \begin{bmatrix} V_{k,1} & 0 & \cdots & 0 \\ 0 & V_{k,2} & \cdots & 0 \\ \vdots & \vdots & \ddots & \vdots \\ 0 & 0 & \cdots & V_{k,N} \end{bmatrix}$$

where $V_{k,n}$ is the variance of $v_{k,n}$.

The number of measurements is used as a tuning parameter. A larger N increases the observability and tolerance to noise by providing a over-determined set of equations. It also increases the area of the performance function to which the gradient and Hessian are fit. For a performance function in which the Hessian changes as a function of position, a too-large N may slow convergence.

IV. One-Dimensional Example

A one-dimensional example of the method is presented in this section. Consider the problem presented in [14]. A continuous linear plant model given by

$$A = \begin{bmatrix} 0 & 1 & 0 \\ 0 & 0 & 1 \\ -5 & -9 & -5 \end{bmatrix} \quad B = \begin{bmatrix} 0 \\ 0 \\ 1 \end{bmatrix} \quad C = \begin{bmatrix} 1 & 0 & 0 \end{bmatrix}$$

seeks the extremum of a performance function. In this example the performance function was chosen to be $f(x) = \big(\cos(x/8.4) + 1.5\big)\big(x/6 - 0.4\big)^2$ in place of the quadratic function used in [14]. This performance function provides a gradient and Hessian that change as a function of position. The performance function magnitude measurements were corrupted with Gaussian distributed noise with a standard deviation of 0.1. There was no noise on the position measurements. The system was implemented in a 1.0 Hz fixed-step discrete simulation. The Kalman filter operated at 0.25 Hz. The matrix H_k in equation (8) was selected to have 10 rows. The other elements of equation (8) were selected to be of compatible size. The command filter was set to 1 and the persistent excitation, PE in Figure 1, was set to 0.

An initial command was provided to the plant. As the system responded to the command, position and performance function magnitude measurements were provided to the Kalman filter. Estimates of the gradient and Hessian from the Kalman filter were combined, $x_c = b_k M_k^{-1}$, to command the plant toward the local extremum.

As the system approached the extremum, Δf_k became small and was buried in noise, leading to poor estimates. Typically, the Hessian estimate suffers more than the gradient estimates. To partially compensate for this, the system switched between a steepest-descent approach and a Newton approach. When the smallest singular value of the Kalman filter's error covariance, $\underline{\sigma}(P_k) \leq 0.005$, a Newton approach was used. When $\underline{\sigma}(P_k) > 0.005$, a steepest-descent approach was used. The switching threshold was used as a tuning parameter and selected by trial and error.

The plant position as a function of time is presented in Figure 2. The minimum position is depicted by a solid line and is reached by the system in approximately 80 seconds, after which noisy estimates cause the plant to deviate from the minimum.

The gradient and Hessian estimates are shown in Figure 3. The Kalman filter estimates are represented by dashed lines. The true gradient and Hessian are represented by solid lines. The system required three measurements before beginning estimation, thus, the figures show the first non-zero estimate at 12 seconds. It is apparent that the estimations began to suffer once the system neared the minimum. If the simulation were allowed to execute for a longer time period, position would have randomly moved about the minimum. This example illustrated application of the method to a simple one-input one-ouput problem. The gradient and Hessian estimates track the true values well and the system quickly reaches the extremum. The next example illustrates the natural extension of the method to multiple-input problems.

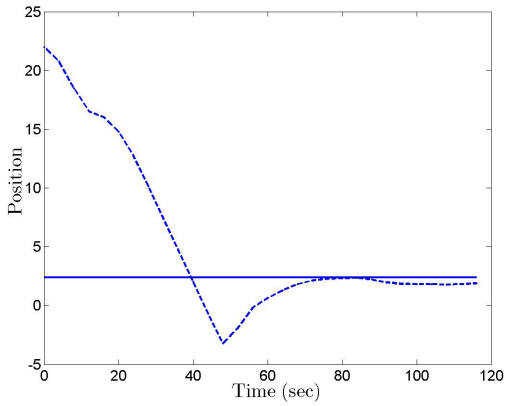

Fig. 2. Plant position versus time. Dashed line: Plant position. Solid line: Performance function minimum.

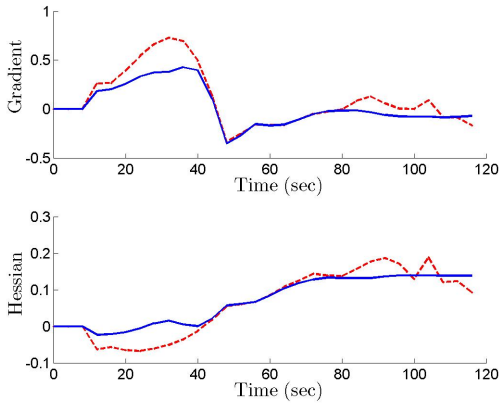

Fig. 3. Estimated and true gradient and Hessian versus time. Dashed line: Kalman filter estimates. Solid line: True gradient and Hessian.

V. Two-Dimensional Example

A two-dimensional example of the scheme is presented in this section. Consider the problem of formation flight for drag reduction. In this problem, a trailing aircraft attempts to fly its wingtip in the wingtip vortex of a leading aircraft to reduce the induced drag. Substantial fuel savings can be achieved by employing such a technique.

This problem has been studied in multiple papers. A formation of two Dornier Do 28-D1 aircraft has been flown under automatic control achieving 15% flight power reduction [17], and two F/A-18 aircraft have achieved 20% drag reduction and 18% fuel flow reduction [18]. More details of formation flight including theoretical derivations of the drag reduction achievable in formation flight can be found in [1] and [17].

In this example, a two-ship formation of transport class aircraft is modeled and a peak-seeking control system is designed to maximize drag reduction. It is assumed that the lead aircraft flies in a straight-and-level path. This allows the vortex generated by the lead aircraft to be modeled as static maps of induced drag coefficient and rolling moment on the trailing aircraft as a function of lateral and vertical relative position. The induced drag coefficient map is used as the performance function. The magnitude of the rolling moment map for any given position is used as a disturbance input to the trailing aircraft model. The maps were generated using a vortex-lattice method with the trailing aircraft wingtip positioned inside the leading aircraft wingtip vortex. For each position of the map, the aircraft was first trimmed for straight-and-level flight and then the induced drag coefficient and rolling moment were calculated. It is assumed that the vortex changes little with respect to relative longitudinal spacing.

The trailing aircraft is modeled with an 11-state, 4-input, 10 Hz discrete state-space model. The modeled states are body-axis vertical, lateral, and longitudinal velocities; roll, pitch, and yaw angles; roll, pitch, and yaw rates; and inertial-axis lateral and vertical relative positions between aircraft. The inputs are elevator deflection, aileron deflection, rudder deflection, and thrust. The effects due to a changing induced drag coefficient are not modeled.

Normally distributed random noise with a standard deviation of 0.001 is superimposed on the induced drag coefficient performance function magnitude. In addition, normally distributed random noise with a standard deviation of 0.012 meter is superimposed on the position measurements.

A. Inner-Loop Control Design

The primary goal of the inner-loop control law is to move the trailing aircraft to track relative vertical and lateral position commands between the leading and trailing aircraft. The secondary goal is to minimize roll angle to ensure the trailing aircraft wing remains in the vortex during lateral movement. The third goal is to maintain a constant relative longitudinal velocity to prevent the trailing aircraft from slowly drifting out of formation.

In order to meet these goals, an inner-loop control system was designed which penalizes roll angle and change in longitudinal velocity. It follows relative lateral and vertical position commands by commanding elevator, rudder, aileron, and thrust. An LQR-tracker control design methodology was selected for construction of the control system. The aircraft model was augmented with integral states of the lateral position error, vertical position error, longitudinal velocity command, and roll angle. Controller gains were computed by minimizing the standard LQR cost function

$$\int_0^\infty x^T Q x + u^T R u \, \mathrm{d}t \tag{9}$$

where Q and R are designer selected weightings on the states, x, and inputs, u, respectively. The resulting gains were used in the interconnection shown in Figure 4. In the figure, h

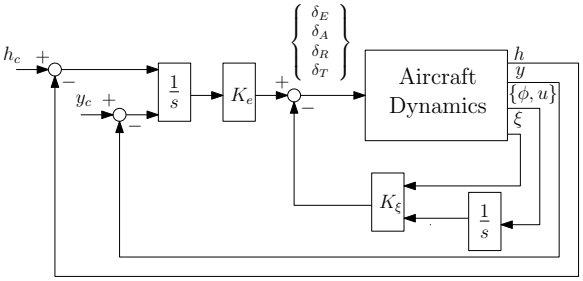

Fig. 4. Inner-loop-control-system interconnection.

represents vertical relative position, y lateral relative position, ϕ roll angle, and u longitudinal velocity. Vertical, lateral, and longitudinal velocities; roll, pitch, and yaw angles; and roll, pitch, and yaw rates are contained in ξ. Elevator deflection is represented by δ_E, aileron deflection by δ_A, rudder deflection by δ_R, and thrust by δ_T. Control gains on the aircraft states are represented by K_ξ, and control gains on the errors by K_e. The subscript c on the loop inputs indicates a command to the system.

B. Kalman Filter Design

A Kalman filter was designed as discussed in section III above. It was chosen to iterate at 0.1 Hz to allow the aircraft to travel some distance between iterations. Measurements were taken at 10 Hz in between the iterations and averaged to form $f_{k,n}$, $x_{1_{k,n}}$, and $x_{2_{k,n}}$ of (7). The Kalman filter rate was used as a tuning parameter and selected by trial and error. The matrix H_k in equation (8) was selected to have 15 rows ($N = 15$). The other elements of equation (8) were selected to be of compatible size.

A persistent excitation was chosen as a 3 rad/sec 0.7 meter sinusoidal signal superimposed on the relative-position command. This allowed N values of $f_{k,n}$, $x_{1_{k,n}}$, and $x_{2_{k,n}}$ to be distributed over a full excitation period.

The command filter was chosen to be an 10 Hz integrator, Filt $= 0.1/(z-1)$. This resulted in a ramping position command in place of the step command generated by the 0.1 Hz Kalman filter estimates. In addition, the system was implemented to switch between a steepest-descent and a

Newton approach. When the Hessian estimate was positive definite and the minimum singular value of the Kalman filter error covariance $\underline{\sigma}(P_k) < 6$ a Newton approach was used. Gradient descent was used when this was not the case. The switching threshold was used as a tuning parameter and selected by trial and error.

C. Simulation Results

The system was tested by simulation. In the simulation, the aircraft was initially positioned to the left and above the leading aircraft right wingtip vortex core. Figure 5 depicts the path the aircraft followed during the peak-seeking simulation. The contours represent induced drag coefficient. The system was initially commanded to trace a 0.7 meter radius circle to generate initial gradient and Hessian estimates. It was then allowed to move toward the minimum. The system primarily moved orthogonally through the contours of the plot as it moved to the minimal location. The system reached the local minimum in 300 seconds.

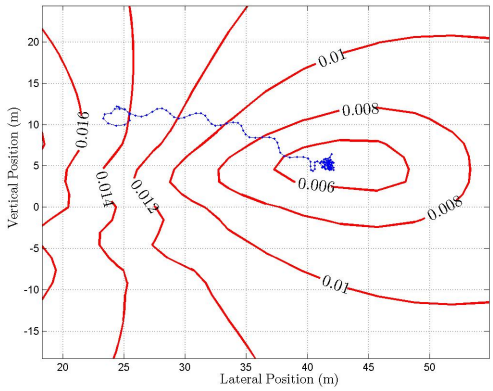

Fig. 5. Aircraft path along induced drag coefficient performance function.

Figures 6 and 7 show the gradient and Hessian estimates as a function of time. The solid lines in the figures represent the true gradient and Hessian while the dashed lines represent the estimates at each Kalman filter iteration. The gradient estimate approximates the true gradient well over the length of the entire simulation, as shown in Figure 6; however, the Hessian estimate illustrated in Figure 7 is less accurate.

The error between position commands and the aircraft response is depicted in Figure 8. The error never exceeds 0.8 meters. The oscillatory behavior is due to the excitation command.

The aircraft Euler angles are depicted in Figure 9. The aircraft angles stay within reasonable values, never exceeding 5 degrees. The high-frequency oscillatory appearance of the angles is due to non-smooth commands being provided to the aircraft. Improvement to the command filter could minimize these oscillations. The slower-period oscillations are due to the excitation. The roll and yaw angles share the task of moving the aircraft laterally. By changing the weightings contained in R of the inner-loop control design (9), surface movements can be tuned to use more roll or yaw angle.

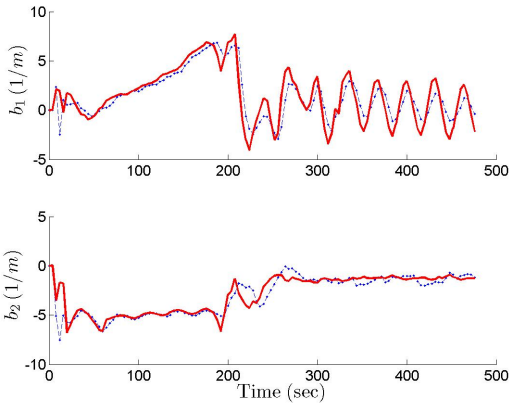

Fig. 6. Gradient estimates and true gradient. Solid line: truth. Dots: Estimate.

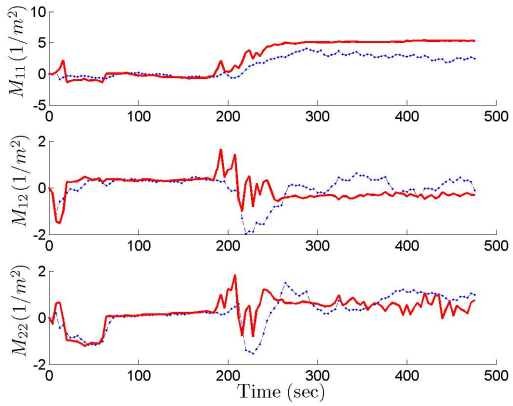

Fig. 7. Hessian estimates and true Hessian. Solid line: Truth. Dots: Estimate.

The aircraft surface deflections are displayed in Figure 10. As with the Euler angles, the high-frequency oscillation is due to the non-smooth commands to the aircraft and the slower oscillation is due to the excitation. Aileron deflection goes to 10 degrees and rudder deflection goes to 5 degrees when the aircraft is tracing the initially-commanded circle. The simulation ends with all surface deflections except aileron near 0. Aileron deflection remains at 3 degrees because the aileron continues to counteract the vortex-induced rolling moment.

This example has demonstrated the application of the method to a two-input one-output problem. The method can also be applied to problems with larger numbers of inputs; however, the number of estimation parameters grows with the number of inputs, m, as $\sum_{i=1}^{m} i + m$. The estimation problem then demands a larger number of measurments, N.

VI. Conclusion

A parametric peak-seeking control technique has been presented. It utilizes a linear time varying Kalman filter to directly use coordinate and magnitude measurements of the performance function to estimate the gradient and Hessian. The Kalman filter is developed from a Taylor

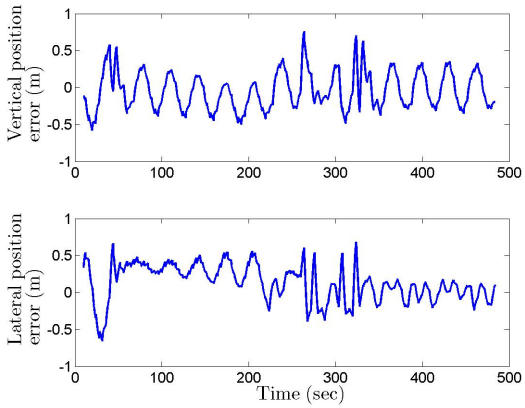

Fig. 8. Vertical and lateral position errors.

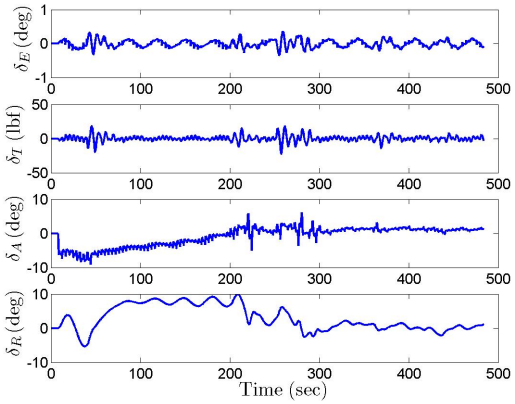

Fig. 10. Aircraft surface deflections versus time.

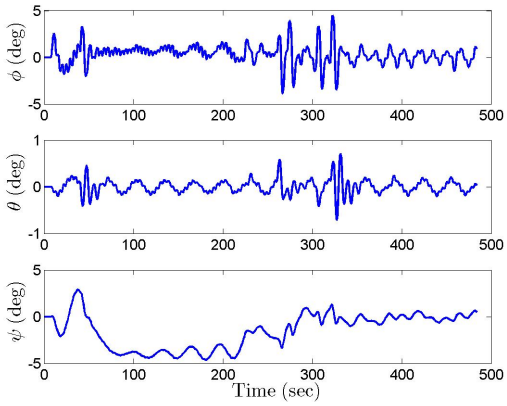

Fig. 9. Aircraft Euler angles versus time.

series approximation of the performance function about the current coordinate measurement. It uses the difference between subsequent measurements of position and performance function magnitude. The estimates are used in a Newton method optimization approach to drive the plant toward the performance function extremum. Both a one-dimensional and a two-dimensional example are provided to illustrate the technique. Both demonstrate good results. In the one-dimensional example, the scheme reaches the minimum in 80 seconds and displays good gradient and Hessian estimates while using noisy performance function magnitude measurements. Application to a two-dimensional problem is exhibited with the problem of formation flight for drag reduction. In this example, the minimum is reached in 300 seconds and exhibits good gradient and Hessian estimates. This example used noisy performance function magnitude and coordinate measurements. The flexibility of the linear time-varying Kalman filter allows applicability of the method to a large number of problems.

REFERENCES

[1] D. Chichka, J. Speyer, C. Fanti, and C. Park, "Peak-Seeking Control for Drag Reduction in Formation Flight," *J. Guid. Control Dyn.*, vol. 29, no. 5, pp. 1221–1230, September-October 2006.

[2] H.-H. Wang and M. Krstic, "Optimizing bioreactors by extremum seeking." [Online]. Available: citeseer.ist.psu.edu/182943.html

[3] H. Wang, S. Yeung, and M. Krsti'c, "Experimental application of extremum seeking on an axial-flow compressor," 1998. [Online]. Available: citeseer.ist.psu.edu/wang98experimental.html

[4] C. S. Draper and Y. J. Li., "Principles of optimalizing control systems and an application to an internal combustion engine," *ASME Publications*, September 1951.

[5] I. I. Ostrovskii, "Extremum regulation," *Automatic and Remote Control*, vol. 18, pp. 900–907, 1957.

[6] P. F. Blackman, "Extremum-seeking regulators," *in J. H. Westcott, Ed., An Exposition of Adaptive Control*, The Macmillan Company 1962.

[7] O. L. R. Jacobs and G. C. Shering, "Design of a single-input sinusoidal-perturbation extremum-control system," *Proceedings IEE*, vol. 115, pp. 212–217, 1968.

[8] D. Popovic, M. Jankovic, S. Magner, and A. Teel, "Extremum seeking methods for optimization of variable cam timing engine operation," *IEEE Transactions on Control Systems Technology*, vol. 14, no. 3, pp. 398–407, 2006.

[9] E. Lavretsky, N. Hovakimyan, A. Calise, and V. Stepanyan, "Adaptive vortex seeking formation flight neurocontrol," in *in AIAA Guidance, Navigation, and Control Conference and Exhibit*, pp. 11–14.

[10] K. Ariyur and M. Krstic, *Real-Time Optimization by Extremum-Seeking Control*. Wiley-IEEE, 2003.

[11] C. Zhang and R. Ordonez, "Numerical Optimization-based Extremum Seeking Control of LTI Systems," *Decision and Control, 2005 and 2005 European Control Conference. CDC-ECC'05. 44th IEEE Conference on*, pp. 4428–4433, 2005.

[12] K. Ariyur and M. Krstic, "Analysis and design of multivariable extremum seeking," *American Control Conference, 2002. Proceedings of the 2002*, vol. 4, 2002.

[13] M. Krstic and H.-H. Wang, "Extremum seeking feedback: Stability proof and application to an aeroengine compressor model." [Online]. Available: citeseer.ist.psu.edu/krstic98extremum.html

[14] F. Najson and J. Speyer, "Extremum seeking loop for a class of performance functions," in *15th IFAC World Congress on Automatic Control*, Barcelona, Spain, July 2002.

[15] R. Brown and P. Hwang, *Introduction to Random Signals and Applied Kalman Filtering: With MATLAB Exercises and Solutions*. Wiley, 1997.

[16] M. Grewal and A. Andrews, *Kalman Filtering: Theory and Practice Using MATLAB*. Wiley, 2001.

[17] M. Beukenberg and D. Hummel, "Aerodynamics, performance and control of airplanes in formation flight," in *17th Congress of the International Conclil of the Aeronautical Sciences ICAS 1990*, 1990.

[18] M. J. Vachon, R. J. Ray, K. R. Walsh, and K. Ennix, "F\A-18 aircraft performance benefits measured during the autonomous formation flight project," in *the AIAA Guidance, Navigation and Control Conference*, 2002, pp. 2002–4491.

Peak-Seeking Control Using Gradient and Hessian Estimates

Jack Ryan and Jason Speyer

Peak Seeking Control

- Given
  - Performance function
    - Unknown location, magnitude of extremum
  - Measurements
    - Noisy coordinates
    - Noisy magnitude
  - Known plant
- Find
  - Extremum of performance function in real-time

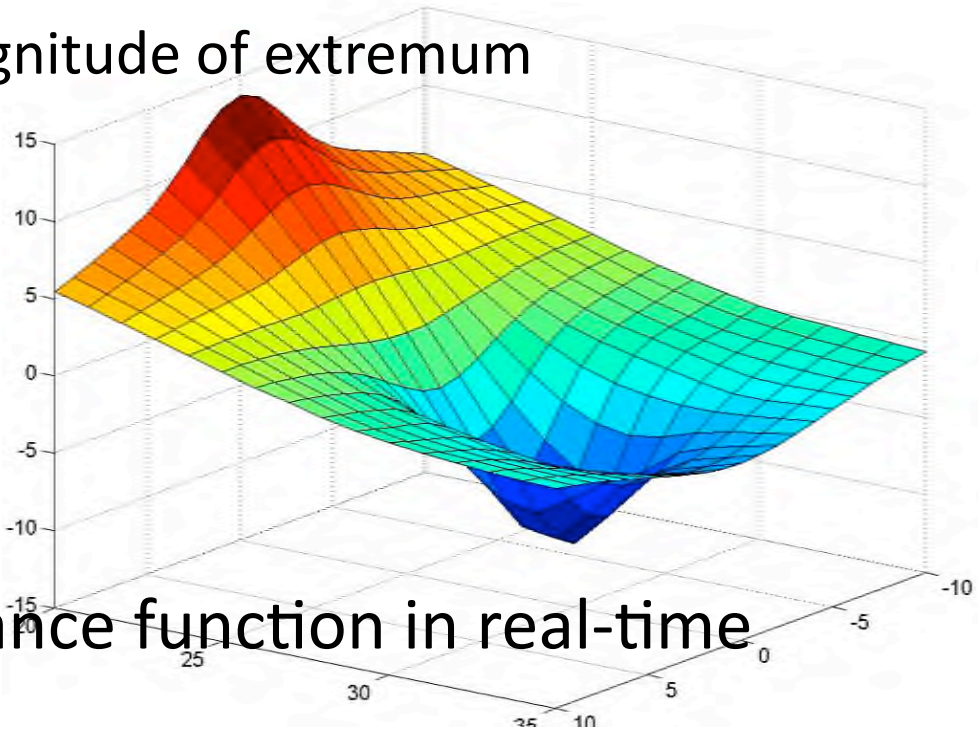

Example Application

- Formation flight for drag reduction
  - Goal: Position trailing aircraft to achieve optimal drag reduction.
  - Extremum position unknown
  - Can measure relative position, magnitude of drag reduction

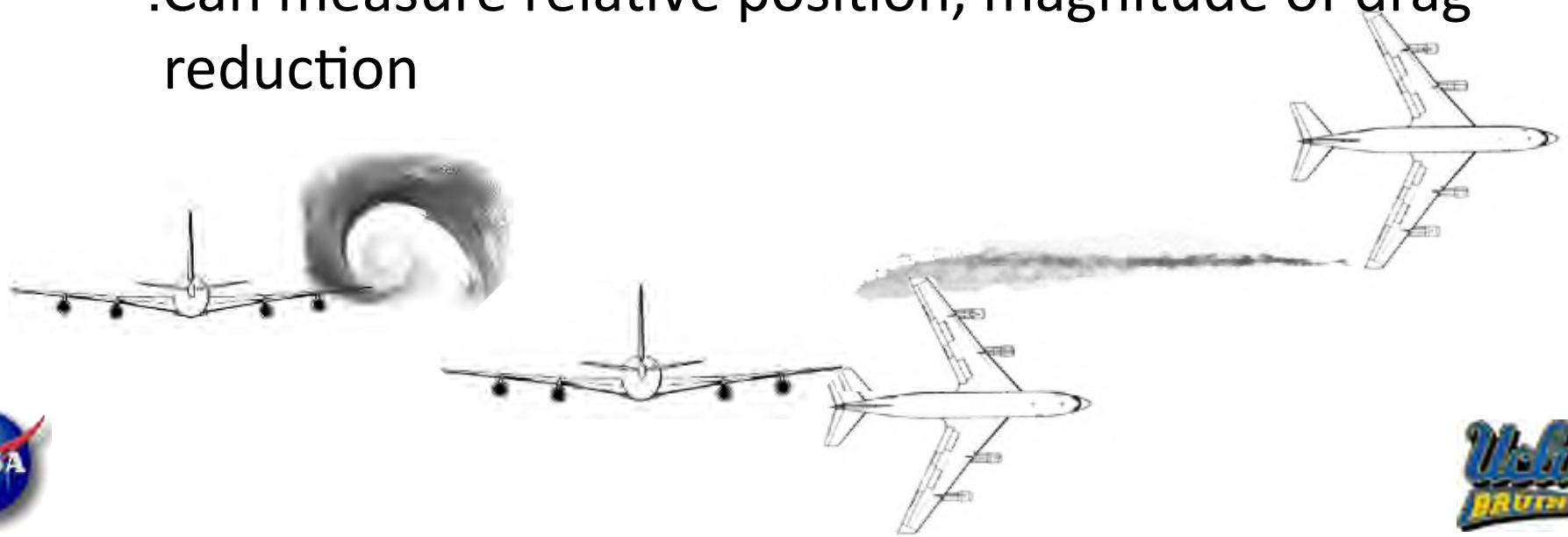

Overview of scheme

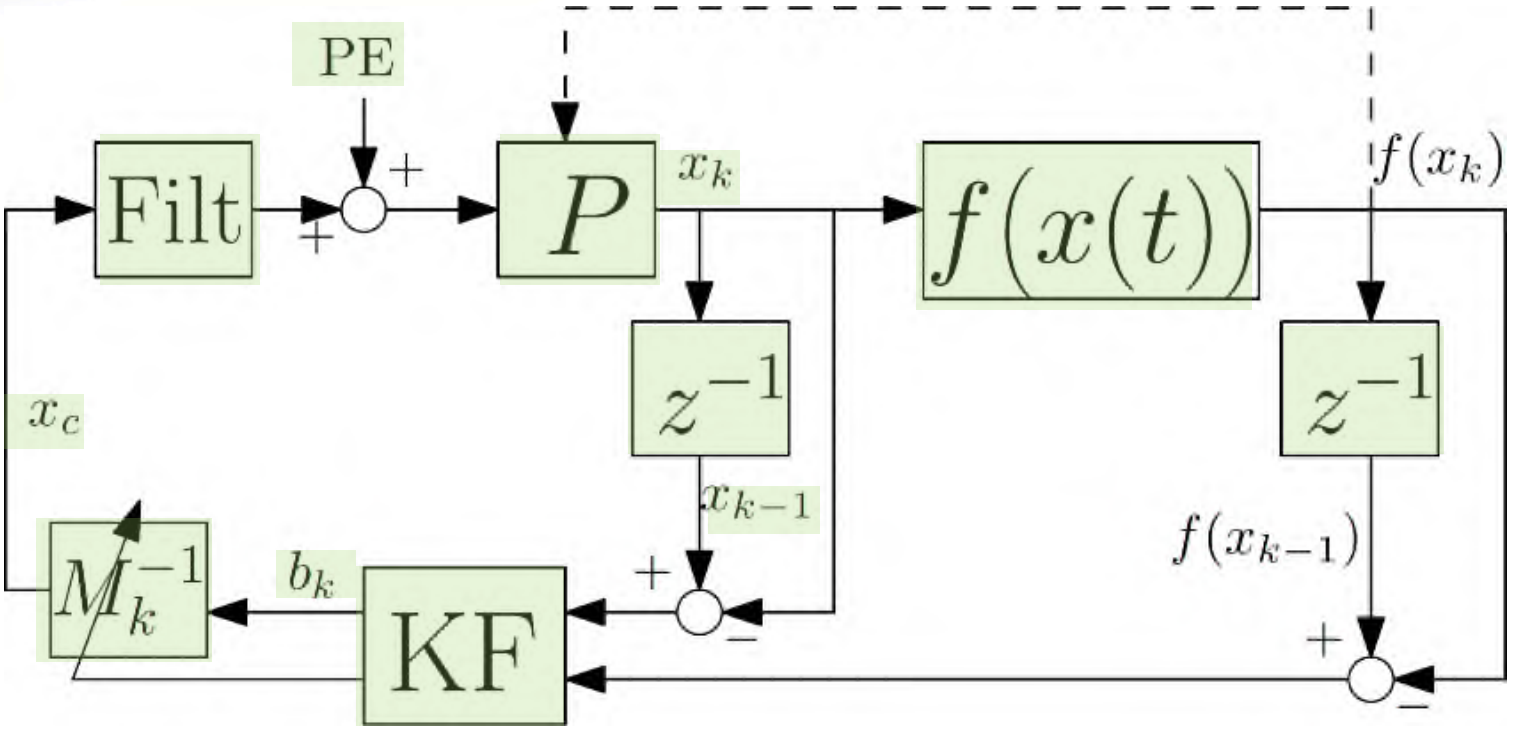

Performance function	$f(x(t))$
Plant	P
Kalman Filter	KF
Filter	Filt
Position	x_k

Position command	x_c
Gradient estimate	b_k
Hessian estimate	M_k
Persistent Excitation	PE
Delay operator	z^{-1}

Assumptions

- Performance function has single extremum
- Measureable coordinates and magnitude
- Gausian distributed noise
- Plant is stable and controllable
  - Inner loop control design treated as separate problem

Kalman Filter construction

- Given

$$\begin{aligned} \zeta_{k+1} &= F_k \zeta_k + \Gamma_k w_k \\ z_k &= H_k \zeta_k + v_k \end{aligned}$$

- Time Varying Kalman Filter

$$\begin{aligned} K_k &= M_k H_k^T \left[H_k M_k H_k^T + V_k \right]^{-1} \\ \hat{\zeta}_k &= \bar{\zeta}_k + K_k \left(z_k - H_k \bar{\zeta}_k \right) \\ P_k &= \left(I - K_k H_k \right) M_k \\ \bar{\zeta}_{k+1} &= F_k \hat{\zeta}_k \\ M_{k+1} &= F_k P_k F_k^T + \Gamma_k W_k \Gamma_k^T \end{aligned}$$

Kalman Filter Measurement Eq.

Taylor Series expansion of PF

$$f(x) \approx f(x_k) + b_{x_k}^T (x - x_k) + \frac{1}{2}(x - x_k)^T M_{x_k}(x - x_k) + o(x - x_k)$$

Assume Quadratic

$$\Delta f_k = b_k^T \Delta x_k + \frac{1}{2}\Delta x_k^T M_{x_k} \Delta x_k$$

Kalman Filter Measurement Eq.

Using multiple measurements

$$\begin{bmatrix} \Delta f_{k,1} \\ \Delta f_{k,2} \\ \vdots \\ \Delta f_{k,N} \end{bmatrix} = H_k \zeta_k + \begin{bmatrix} v_{k,1} \\ v_{k,2} \\ \vdots \\ v_{k,N} \end{bmatrix}$$

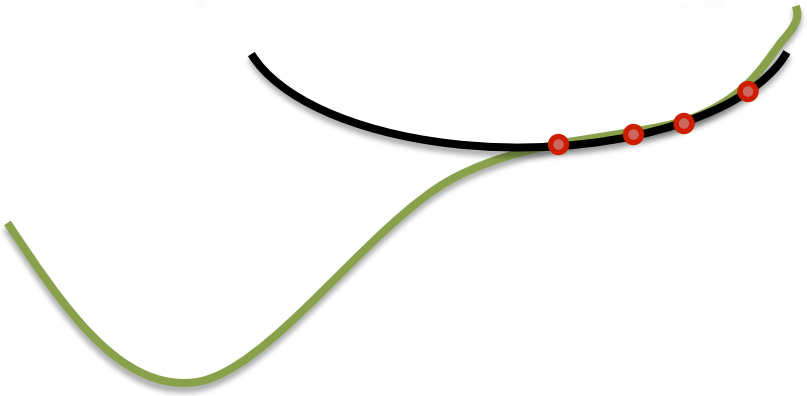

Improves observability

Improves tolerance to noise

Kalman Filter State Eq.

Assume:

Gradient and Hessian change according to Brownian motion

$$\zeta_{k+1} = I\zeta_k + w_k$$

Kalman Filter implemented as:

$$\hat{P}_{k+1} = \bar{P}_k + W_k$$
$$\zeta_{k+1} = \zeta_k + \bar{P}_k H_k^T V_k^{-1}(\Delta f_k - H_k \zeta_k)$$
$$\bar{P}_k = (\hat{P}_k^{-1} + H_k^T V_k^{-1} H_k)^{-1}$$

Formation Flight Application

Transport Class Aircraft

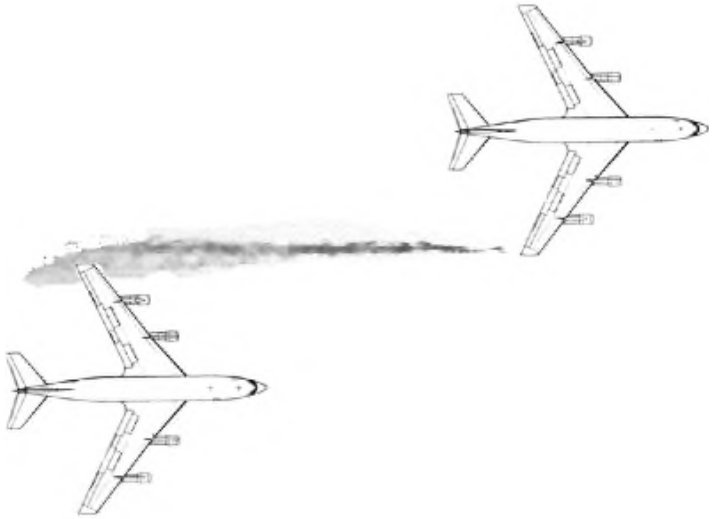

Constraints:

- Smooth response by aircraft
  - Minimize roll angle (use rudder for lateral positioning
  - Slow and small persistent excitation
- Noisy measurements

Inner Loop Control

- ! LQR-tracker design

$$\int_0^{\infty} x^T Q x + u^T R u \, dt$$

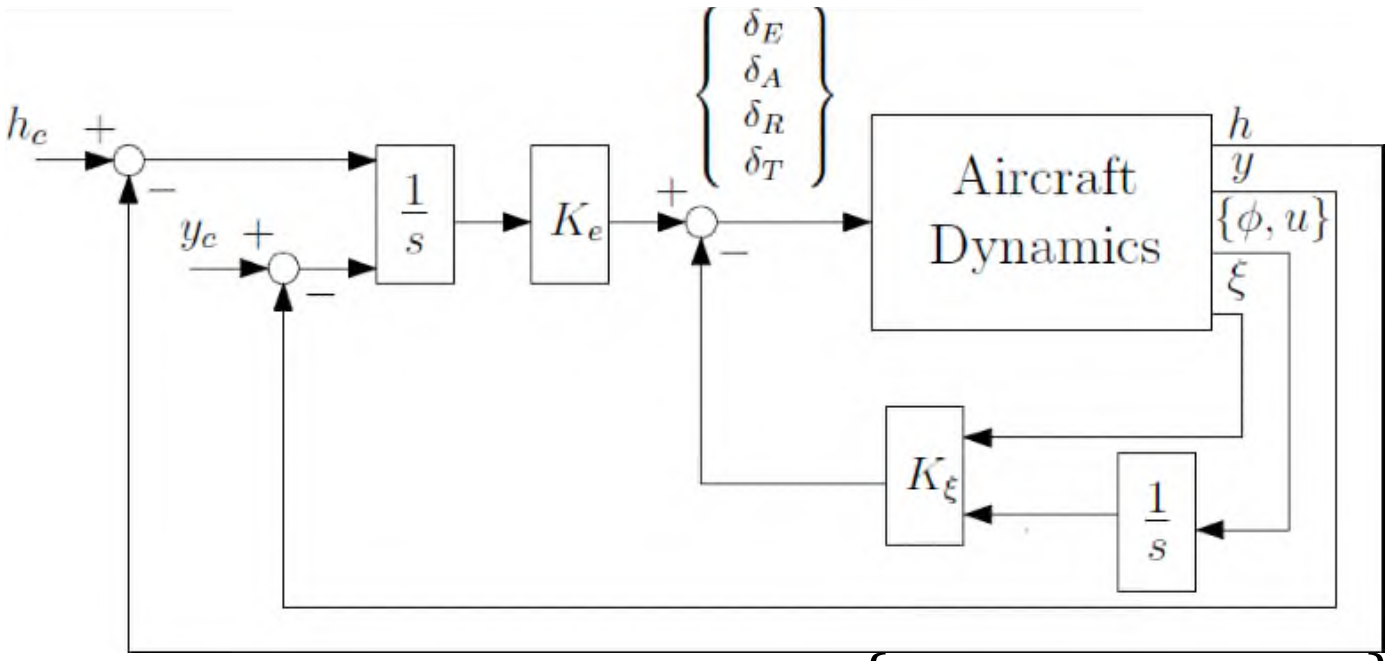

$$\xi = \{u, v, w, \theta, \phi, \psi, p, q, r\}$$

Kalman Filter Design

- ! Induced Drag Coefficient Performance Function
  - !Two-input one-output

$$x_k \in R^{1\times 2}$$

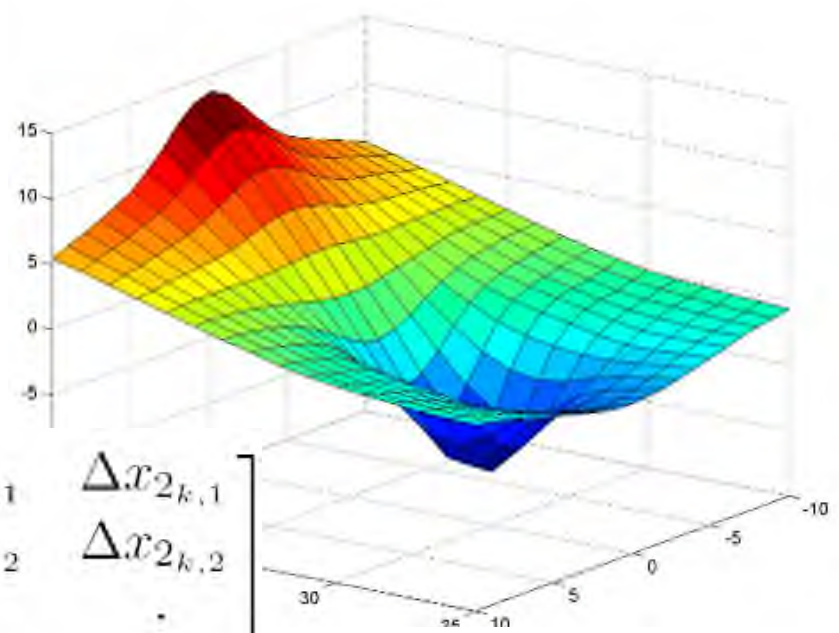

$$H_k = \begin{bmatrix} \frac{1}{2}\Delta x^2_{1_{k,1}} & \frac{1}{2}\Delta x^2_{2_{k,1}} & D_{k,1} & \Delta x_{1_{k,1}} & \Delta x_{2_{k,1}} \\ \frac{1}{2}\Delta x^2_{1_{k,2}} & \frac{1}{2}\Delta x^2_{2_{k,2}} & D_{k,2} & \Delta x_{1_{k,2}} & \Delta x_{2_{k,2}} \\ \vdots & \vdots & \vdots & \vdots & \vdots \\ \frac{1}{2}\Delta x^2_{1_{k,N}} & \frac{1}{2}\Delta x^2_{2_{k,N}} & D_{k,N} & \Delta x_{1_{k,N}} & \Delta x_{2_{k,N}} \end{bmatrix}$$

$$D_{k,n} = \Delta x_{1_{k,n}} \Delta x_{2_{k,n}}$$

Kalman Filter Design

- Iterates at 0.1 Hz
  - Provide change in magnitude in between measurements
- KF using 15 measurements ($H_k \in R^{15\times5}$)
  - Tradeoff between improving noise characteristics and slower convergence
- PE=3 rad/sec 0.7 m sinusoid
  - Minimizes passenger discomfort while providing observability
- $\text{Filt} = 0.1/(z-1)$

Peak Seeking Results

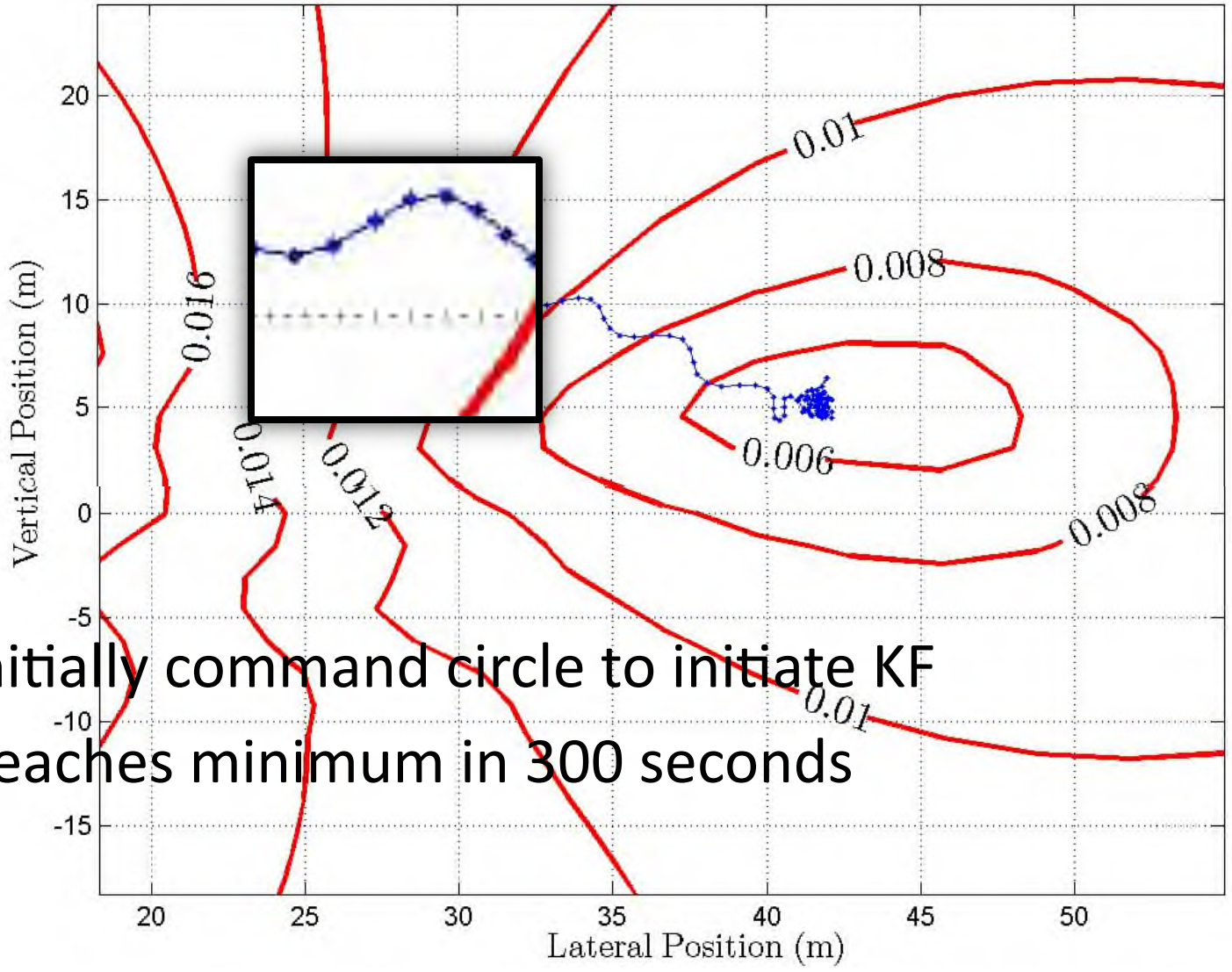

- Initially command circle to initiate KF
- Reaches minimum in 300 seconds

Gradient Estimation

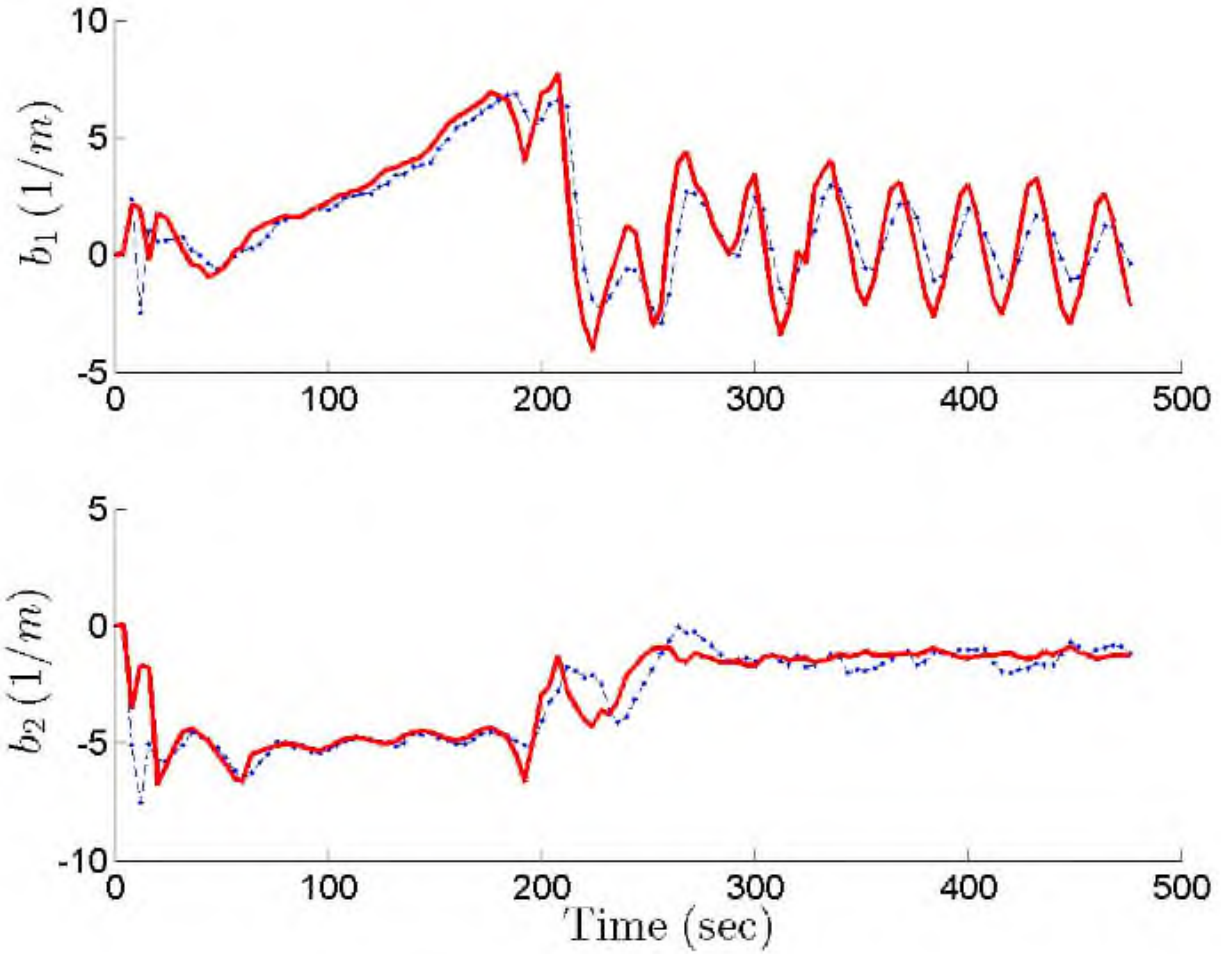

Hessian Estimation

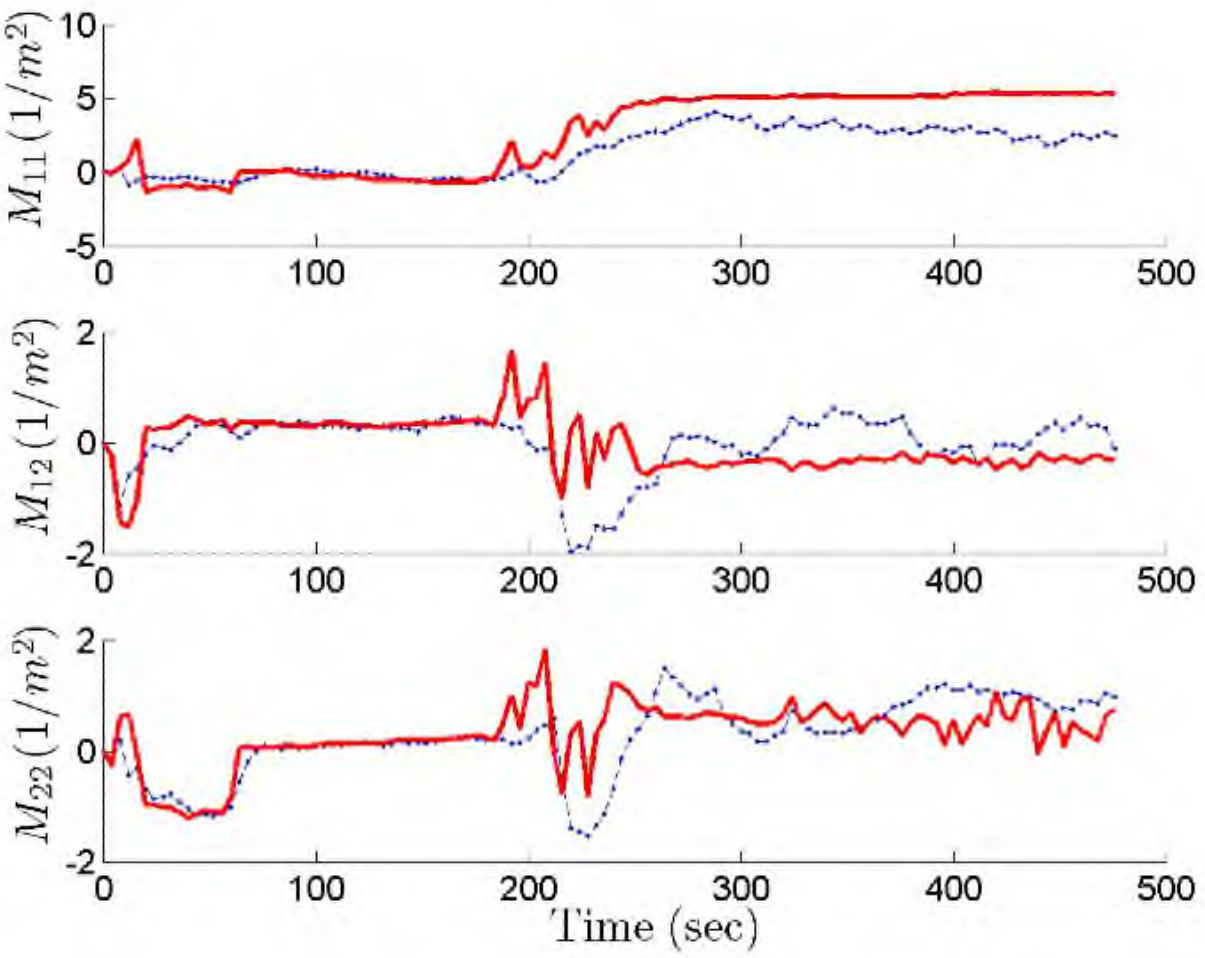

Aircraft response

- ! Roll angle kept under 4 degrees
- ! Yaw angle reaches 5 degrees

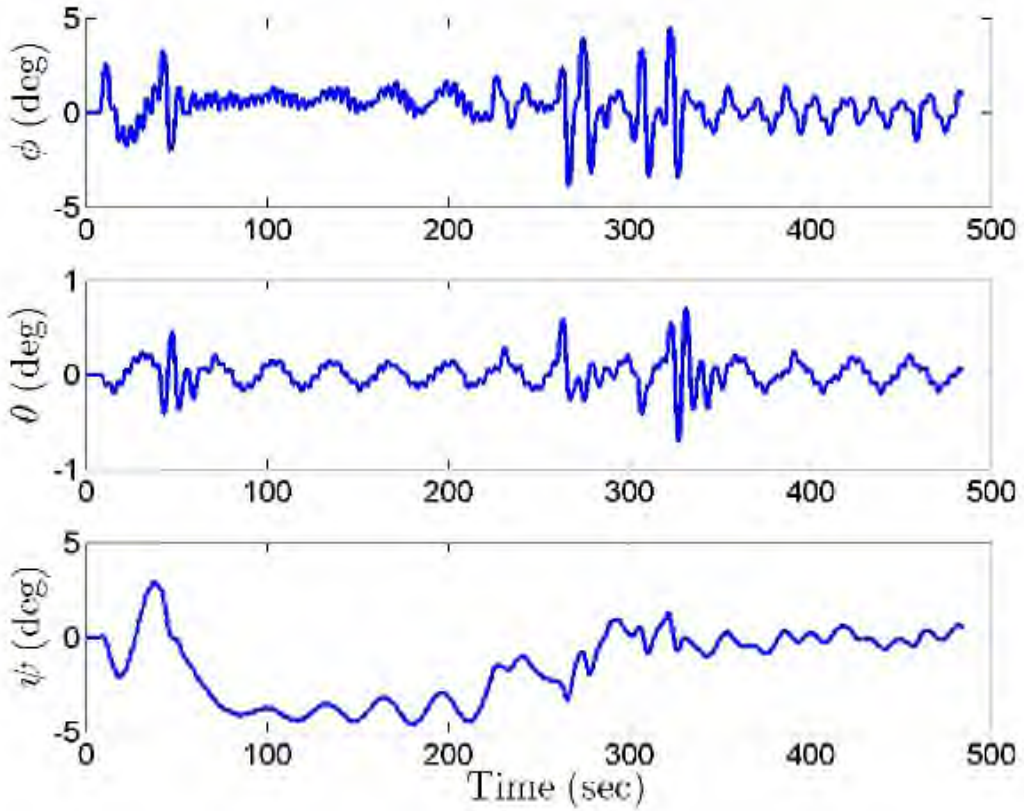

Aircraft Response

- ! Aileron deflection reaches 9 degrees
- ! Rudder deflection reaches 10 degrees